6-2019

Real time HABs mapping using NASA Glenn hyperspectral imager

Reid W. Sawtell
Michigan Technological University, rwsawtel@mtu.edu

Robert Anderson
NASA Glenn Research Center

Roger Tokars
NASA Glenn Research Center

John D. Lekki
NASA Glenn Research Center

Robert Shuchman
Michigan Technological University, shuchman@mtu.edu

See next page for additional authors

Recommended Citation

Authors

Reid W. Sawtell, Robert Anderson, Roger Tokars, John D. Lekki, Robert Shuchman, Karl Bosse, and Michael Sayers

Real time HABs mapping using NASA Glenn hyperspectral imager

Reid W. Sawtell [a,*], Robert Anderson [b], Roger Tokars [b], John D. Lekki [b], Robert A. Shuchman [a], Karl R. Bosse [a], Michael J. Sayers [a]

[a] Michigan Tech Research Institute, Michigan Technological University, 3600 Green Court, Suite 100, Ann Arbor, MI 48105, USA
[b] NASA Glenn Research Center, 21000 Brookpark Road, Cleveland, OH 44135, USA

ARTICLE INFO

ABSTRACT

The hyperspectral imaging system (HSI) developed by the NASA Glenn Research Center was used from 2015 to 2017 to collect high spatial resolution data over Lake Erie and the Ohio River. Paired with a vicarious correction approach implemented by the Michigan Tech Research Institute, radiance data collected by the HSI system can be converted to high quality reflectance data which can be used to generate near-real time (within 24 h) products for the monitoring of harmful algal blooms using existing algorithms. The vicarious correction method relies on imaging a spectrally constant target to normalize HSI data for atmospheric and instrument calibration signals. A large asphalt parking lot near the Western Basin of Lake Erie was spectrally characterized and was determined to be a suitable correction target. Due to the HSI deployment aboard an aircraft, it is able to provide unique insights into water quality conditions not offered by space-based solutions. Aircraft can operate under cloud cover and flight paths can be chosen and changed on-demand, allowing for far more flexibility than space-based platforms. The HSI is also able to collect data at a high spatial resolution (~1 m), allowing for the monitoring of small water bodies, the ability to detect small patches of surface scum, and the capability to monitor the proximity of blooms to targets of interest such as water intakes. With this new rapid turnaround time, airborne data can serve as a complementary monitoring tool to existing satellite platforms, targeting critical areas and responding to bloom events on-demand.

Introduction

Harmful algal blooms of cyanobacteria (cyanoHABs) commonly grow in aquatic environments throughout the world, including fresh-water bodies within the Great Lakes Basin (Bianchi et al., 2000; Vahtera et al., 2007; Joehnk et al., 2008; Qin et al., 2010; Schindler et al., 2012). Water bodies that have abundant or excessive nutrients such as nitrogen and phosphorus support the rapid growth or blooming of cyanobacteria (Robarts and Zohary, 1987; Rapala et al., 1997; Ibelings et al., 2003; Kanoshina et al., 2003; Paerl et al., 2011). The blooms that occur in the Great Lakes often float on the surface as a mat of blue-green scum, but can also be mixed throughout the water column (Rowe et al., 2016; Sayers et al., 2016; Bosse et al., this issue). In addition to being stimulated by nutrients, bloom formation and vertical distribution are affected by water temperature, wind, waves, and currents (Wynne et al., 2010; Stumpf et al., 2012; Rowe et al., 2016; Sayers et al., 2016). Blooms with a significant surface scum component often occur during periods of hot air, warm water surface temperature, and relatively calm winds (van Rijn and Shilo, 1985; Klemer et al., 1996).

Some blooms of cyanobacteria produce toxic compounds (cyanotoxins) which can harm animal and human health (Sivonen, 1996; Codd et al., 2005). Incidents of cyanoHABs have been increasing in some regions across North America (Urquhart et al., 2017) including in the Great Lakes Basin (Stumpf et al., 2012; Sayers et al., 2016), where the most common cyanotoxins include microcystin (liver toxin), cylindrospermopsin (liver and dermatoxin), and anatoxin-a (neurotoxin) (Boyer, 2007). Ingestion of, or exposure to, water polluted by cyanotoxins has adverse health effects which is a problem for both recreational and drinking water supplies; thus there is a need for a cost-effective and timely monitoring procedure.

Because of the highly dynamic nature of cyanoHAB events (Jetoo et al., 2015; Lekki et al., this issue), the rapid dissemination of extent and severity information is greatly desired. There are several water intakes in Lake Erie that provide drinking water to more than one million people. Real-time knowledge of the proximity of cyanoHAB occurrence to these intakes is critical for water treatment managers to take action mitigating the threat of exposing harmful water to their residents. Similarly, hundreds of recreational and commercial fisherman utilize Lake Erie (Melstrom and Lupi, 2013), and they could benefit by knowing the precise location of blooms so as to make better choices where to operate. A turnaround time of 24 h or less is necessary to be useful to the stakeholders.

* Corresponding author.
E-mail address: rwsawtel@mtu.edu (R.W. Sawtell).

The near-real time (~24 h) delivery of cyanoHAB monitoring data, whether it be in situ measurements or remote sensing observations, is a significant challenge. It is time consuming and cost prohibitive to make in situ water quality measurements at the spatial and temporal scales (i.e., basin-wide within 24 h) needed to provide near-real time feedback to stakeholders. Remote sensing is an effective tool for monitoring the basin-wide dynamics, but this data must be collected, preprocessed, downloaded, post-processed, and interpreted before it can be disseminated to stakeholders.

Advancements in satellite remote sensing platforms and techniques have allowed for the development and application of cost-effective synoptic information for monitoring cyanoHAB events over large spatial and temporal gradients (Wynne et al., 2008; Stumpf et al., 2012; Wynne and Stumpf, 2015; Sayers et al., 2016; Ho et al., 2017). While the application of satellite remote sensing has been useful to help provide cause and effect linkages between basin-wide cyanoHAB extent and severity (Stumpf et al., 2012; Sayers et al., 2016), the moderate (300 m) to coarse (1 km) spatial resolutions associated with current platforms with near-daily revisit times (i.e., OLCI, the Ocean and Land Colour Instrument and MODIS, the Moderate Resolution Imaging Spectroradiometer) hampers their ability to provide detailed information at small spatial scales. Water treatment managers and recreational users need the information at these small scales to know where cyanoHAB occurrences are located relative to a specific point of interest. There are remote sensing platforms with higher spatial resolution (i.e., Landsat-8, Sentinel-2, and WorldView-2 and 3) that have been shown to be sufficient to adequately estimate chlorophyll-*a* concentrations and monitor algal blooms in small lakes (Beck et al., 2016; Beck et al., 2017). However, these platforms either have an extended revisit time (8 days for the Landsat-7 and 8 constellation, 5 days for the Sentinel-2a and 2b constellation) or are commercial platforms that would require a significant investment for long-term monitoring. These satellite sensors also have limited spectral resolution, limiting the ability to use preferred water quality algorithms such as the Cyanobacteria Index (CI; Stumpf et al., 2012). Aside from spatial and temporal resolution tradeoff issues, satellite platforms are unable to observe the water surface through significant cloud cover, which is quite prevalent in the Great Lakes region (Ackerman et al., 2013; Wynne et al., 2013).

Coinciding with advancements in multispectral satellite remote sensing platforms, many algorithms have been developed to monitor chlorophyll-*a* and harmful algal blooms using multispectral remote sensing retrievals. These algorithms fall into three categories: analytical, semi-analytical (or ratio-based), and derivative (or spectral shape) (Stumpf et al., 2016). Derivative algorithms are least sensitive to atmospheric contamination and have been shown to estimate chlorophyll-*a* which has been found to be a good predictor for phycocyanin, an indicator of cyanobacteria (Stumpf et al., 2016). Research has shown that several chlorophyll-*a* algorithms perform well with airborne imagery to estimate concentrations in inland water bodies (Beck et al., 2016). These include the CI, Maximum Chlorophyll Index (MCI; Binding et al., 2013), Florescence Line Height (FLH; Zhao et al., 2010), Normalized Difference Chlorophyll Index (NDCI; Mishra and Mishra, 2012), 2BDA (Dall'Olmo and Gitelson, 2005), and 3BDA (Gitelson et al., 2003) (Beck et al., 2016). Like the NDCI, the Surface Scum Index (SSI; Sayers et al., 2016) is a variation of the common Normalized Difference Vegetation Index (NDVI). Results from the CI and SSI algorithms are used by NOAA for monitoring harmful algal blooms in western Lake Erie during the cyanobacteria growing season (via the NOAA HAB Bulletin and CoastWatch, respectively).

Airborne remote sensing systems offer several advantages over satellite-based systems to monitor cyanoHAB occurrences at the smaller spatial scales that water resource managers and recreational users find beneficial. Airborne sensing systems are generally flown at relatively low altitudes (<10,000 ft) in conjunction with high resolution camera optics, which produce high spatial resolution (~1–3 m) images of the

ground target. At these resolutions it is possible to resolve cyanoHAB occurrences in localized areas such as docks and marinas as well as near water intake stations. Airborne systems also afford the potential to monitor rivers, bays and small lakes that are not resolvable using daily polar-orbiting satellite platforms for blooms, and their results have been shown to compare well with in situ measurements (Lekki et al., 2009; Beck et al., 2016, 2017). Additionally, airborne platforms can usually provide observations under higher altitude clouds which often obscure images taken by satellite-based platforms.

Airborne remote sensing is not without its own difficulties for near-real time (i.e., within 24 h) water quality monitoring applications. The process of georectifying airborne images can be problematic due to uncertainties in knowing the aircraft's exact location (latitude and longitude) and orientation (pitch, roll, and yaw) at the time of image capture. Careful measurements with a quality Global Positioning System (GPS) and Inertial Navigation System (INS) are required to accurately georectify airborne imagery. (Ortiz et al., 2017) Other issues with using airborne systems for monitoring blooms include that the spatial coverage is limited by lower flying altitudes, making basin-wide monitoring and mapping generally unfeasible. It has also been historically true that the high cost of airborne remote sensing missions (including the costs of planning, acquisition, and processing data) limited the ability to use this method for routine monitoring.

Also critical to producing scientific quality data is the process of atmospheric correction which can complicate the near-real time processing of airborne remote sensing data. Like satellite remote sensing systems, airborne remote sensing observations are often contaminated by atmospheric effects, even at low altitudes, as the atmosphere is very dense close to the Earth's surface (Mobley et al., 2016). Moreover, many areas experiencing cyanoHAB conditions are in close proximity to shore and urbanized locations that contribute varying particle compositions into the atmosphere that must be taken into account. Atmospheric contamination in the signal observed from airborne sensors is a significant problem for algorithms that rely on precise spectral shapes and magnitudes of the water leaving radiance. Atmospheric correction for airborne systems are typically carried out using radiative transfer modeling (e.g. MODTRAN) or empirically using coincident in situ radiometric measurements as reference (Brando and Dekker, 2003; Ortiz et al., 2017). Both of these approaches can also be problematic to incorporate into a near-real time monitoring system. While MODTRAN has been demonstrated to be useful in some scenarios (Brando and Dekker, 2003), it requires rigorous knowledge of atmospheric characteristics such as the aerosol type, water column contents, atmospheric gases, as well as platform altitude. Because these inputs can be highly variable over water, particularly those close to land, it cannot be assumed they are constant, thus making MODTRAN difficult to implement for operational use. Furthermore, no robust aerosol models have been developed for inland waters such as the Great Lakes.

This paper describes the development of a new approach to produce near-real time (i.e. within 24 h) cyanoHAB monitoring products from an experimental Hyper-Spectral Imaging (HSI) system developed and operated by NASA Glenn Research Center (GRC) showing the distribution of cyanoHAB in the Western Basin of Lake Erie (WBLE) as well as surrounding lakes and rivers in northern Ohio. The HSI system is briefly described along with the data processing procedures used to georectify and radiometrically correct the data, including a novel approach of using a nearby parking lot to correct the airborne reflectance signal. The algorithms used to generate the cyanoHAB products are described. Several case studies are also presented to highlight the utility of the new approach with ground truth comparisons for validation.

Methods

The HSI system is a custom-built hyperspectral pushbroom sensor designed by the NASA GRC to be mounted in an aircraft to collect hyperspectral radiance of the earth surface. For this study, the HSI

system was mounted on a Twin Otter aircraft which was flown routinely over western Lake Erie in the summers of 2015, 2016, and 2017. This included 15 flights in 2015 between July 13 and September 18, 14 flights in 2016 between June 6 and October 25, and 10 flights in 2017 between June 21 and October 18. The flight paths were generally targeted to include water intakes and to intersect with in situ sampling locations. Flight paths also included the parking lot at the Maumee Bay State Park for calibration purposes. Example flight paths over western Lake Erie from August 10, 2015 can be seen in Fig. 1, which also shows the ability of the airborne sensor to collect water imagery while the satellite view is obscured by clouds. Targeted overflights of small lakes and rivers were also undertaken, including flights over the Ohio River on September 3, 2015.

The HSI was designed to allow flexible replacement of key components, such as replacing the field-of-view (FOV) lens to modify swath width and cross-track resolution, or to replace other components in order to incorporate system upgrades as they become available. Nominally the system generated pixels that were 1 m in the along-track direction by limiting the rate of image sampling according to the aircraft velocity and altitude. Cross-track pixel width was variable depending on system configuration, e.g. using a 12° optic at an altitude of 3 km would result in a swath width of 658 m and a pixel width of 1 m. The radiance sensor covered the visible wavelengths between 400 and 900 nm at a 2.5 nm spectral resolution. An ASD spectroradiometer with a remote cosine receptor mounted on the top of the aircraft collected downwelling irradiance from 400 to 950 nm which was used to normalize measured radiance into at-sensor reflectance. The aircraft also had an INS and GPS which enabled georeferencing.

The GRC HSI is optimized to measure water-leaving radiances which are typically very low in magnitude compared with other targets on land or in the atmosphere (Mobley et al., 2016). This resulted in terrestrial features within HSI images frequently being saturated in some bands while measurements of aquatic targets usually fell within the dynamic range of the sensor.

The GRC HSI system was calibrated utilizing a NIST traceable Labsphere and a mercury argon calibration lamp. The mercury argon lamp was used to determine the wavelength scale by imaging the lamp outputs with the HSI imager. The Labsphere produced a certified radiance vs wavelength profile which was used to determine a radiance per count image. This calibration image was used after data was collected to convert the sensor output images to radiance. To accommodate for possible shifts in the wavelength calibration in flight, post-processing scripts used the solar "G" and "b" lines (760 and 517 nm, respectively) to check and correct the wavelength calibration if necessary. These shifts are thought to be due to in-flight temperature and pressure changes impacting the sensor geometry. Together, the pre-flight calibration and post-flight adjustments increased the confidence in the quality of the radiance data acquired with the HSI system.

The HSI data was georectified using a ray-tracing technique in which the angular view of each pixel through the fore-optic lens was combined with the roll, pitch, yaw, and GPS coordinate obtained by the system's inertial guidance package (Ortiz et al., 2017). Elevation was assumed to be a constant above-ground-level value, which works well over large bodies of water such as the Great Lakes but limits the georectification accuracy in flights over land.

Utilizing HSI data in a near-real time cyanoHABs monitoring scenario required a number of pre- and post-processing steps as summarized in Fig. 2. Due to the high spatial and spectral resolution, the HSI system generated a substantial volume of data, with each flight track occupying upwards of 30 gigabytes of data and approximately 30 tracks collected per flight. In order to deliver derived products in a timely fashion, the collected data was subjected to a battery of automated processing routines at the NASA GRC that, using the calibration described above, transformed the collected raw data cube into radiometrically calibrated, georeferenced radiance images with supplementary irradiance files. These files were then delivered via FTP to the Michigan Tech Research Institute (MTRI) where the radiance images were converted to at-sensor reflectance and atmospherically corrected using a vicarious
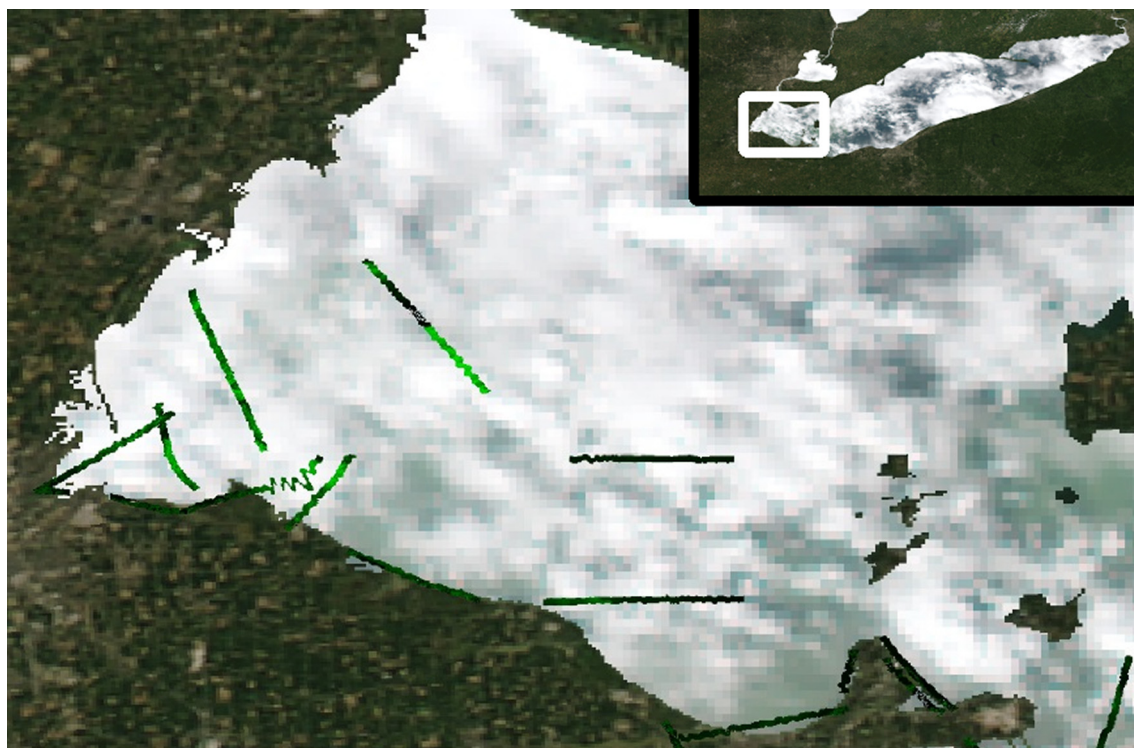
Fig. 1. HSI flight tracks processed with the CI algorithm (horizontal and diagonal lines across the lake) in the Western Basin of Lake Erie overlaid on a true-color image derived from MODIS imagery on the same day (August 10, 2015). Note that the MODIS true-color image is dominated by clouds while the HSI data were obtained under the clouds and are able to indicate areas of significant cyanoHAB presence (shown in green on the flight tracks).
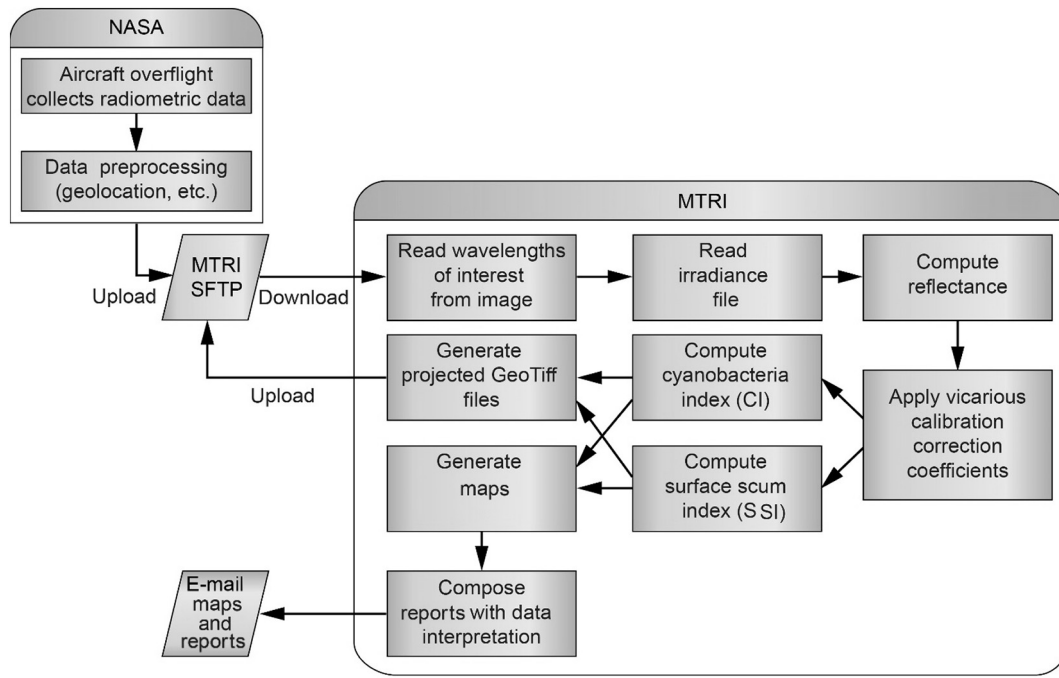
Fig. 2. NASA Glenn Research Center hyperspectral imaging (HSI)data near-real time processing procedure.

empirical line fit correction to generate surface reflectance. The surface reflectance data was then used to compute the CI and SSI products, algorithms routinely used to characterize cyanoHAB events in the Great Lakes. Finally, these derived products were rendered into flight track maps and compiled into reports which were delivered to stakeholders, such as water intake managers, who might incorporate the information into their decision making process.

In order to generate surface reflectance images in near real time to support timely monitoring of cyanoHAB events, a vicarious correction procedure was utilized to account for sensor and environmental (atmospheric) effects. Using a reference target in the image with known surface reflectance, the empirical line fit method (Ortiz et al., 2017) was used to generate a vicarious correction factor to transform at-sensor reflectance to surface reflectance at the reference. This correction factor was then applied to all pixels to generate a surface reflectance image. In this case, the reference target was the Maumee Bay State Park (MBSP) parking lot which offered an optically stable, large, flat, immobile target in close proximity to other areas of interest (i.e. Lake Erie). Coincident with the overflight, measurements of the parking lot were gathered by field crew using a FieldSpec III (ASD, Inc.) spectroradiometer gathering both upwelling radiance and cosine-corrected downwelling irradiance (detailed collection methods will be described later in this section). These values were used in conjunction with the HSI radiance and irradiance observations to produce a correction factor from at-sensor to surface reflectance. The at-sensor reflectance was then multiplied by the correction factor to correct the remaining flight track data under the assumptions that the errors the correction is accounting for do not significantly deviate throughout a given flight and that the parking lot reflectance does not change significantly over time (this assumption is examined in this study).

The wavelength specific correction factors ($C(\lambda)$) were calculated by Eq. (1):

$$C(\lambda) = \frac{Cal_{Ref}(\lambda)}{Uncal_{Ref}(\lambda)} \qquad (1)$$

where $Cal_{Ref}(\lambda)$ is the in situ reflectance of the known target (MBSP

parking lot) and $Uncal_{Ref}(\lambda)$ is the at-sensor reflectance of the target (MBSP parking lot).

This vicarious correction approach allowed for the generation of cyanoHAB maps within 24 h of the flight, meeting the near-real time processing requirement. This simplistic approach performed better than the more complicated and time-consuming MODTRAN-based methods, with the vicarious correction preserving the chlorophyll-a absorption features which were masked out in a MODTRAN (6SV) atmospheric processing algorithm implementation (Lekki et al., 2017). A more detailed comparison of MODTRAN and the vicarious correction approach was outside the scope of this study.

The surface reflectance served as the input to the CI and SSI algorithms. The CI was calculated according to Eq. (2):

$$CI = -\left(Ref(\lambda) - Ref\left(\lambda^M\right) - \left(Ref\left(\lambda^P\right) - Ref\left(\lambda^M\right) \right) \times \frac{\lambda - \lambda^M}{\lambda^P - \lambda^M} \right) \qquad (2)$$

where ref(λ) is the reflectance at λ nanometers and

$\lambda = 679$ nm
$\lambda^M = 664$ nm
$\lambda^P = 709$ nmas described in Stumpf et al. (2012).

The SSI algorithm was calculated using Eq. (3). Lake Erie water typically returns negative NDVI values due to strong pure water absorption in the near-infrared (NIR) wavelengths while surface vegetation returns positive values due to NIR scattering significant enough to mask the pure water absorption. Surface scums are optically similar to any other terrestrial or wetland vegetative growth so a positive response in known water pixels is a reliable indication of scum presence.

$$SSI = \frac{Ref\left(\lambda^N\right) - Ref\left(\lambda^R\right)}{Ref\left(\lambda^N\right) + Ref\left(\lambda^R\right)} > 0 \qquad (3)$$

where ref(λ) is the reflectance at λ nanometers and

$\lambda^R = 667$ nm
$\lambda^N = 858$ nm

The last step in producing the cyanoHAB near real time products was to produce GeoTiff files and colorized maps of the flight tracks for

dissemination to stakeholders. Maps of key features were compiled into a brief report including comments about what is visible in the image including details such as bloom extent, severity, and proximity to critical locations such as water intakes. Algorithmic failures were identified visually and commentary was included on these instances, such as unaccounted atmospheric contamination that occasionally produced spurious indications of CI presence that might be difficult to recognize for end-users unfamiliar with the algorithms and image interpretation techniques.

Coincident with the HSI flights, an extensive field collection campaign took place in 2015 and 2016 in order to provide validation data for the HSI instrument and its derived products. Long-term radiometric data was calculated at the Maumee Bay State Park parking lot in 2017 in order to assess its stability.

The field measurements in 2015 and 2016 included the use of a FluoroProbe III (bbe-Moldaenke GmbH), hereafter referred to as the FluoroProbe, to measure the surface concentration of bluegreen algae as the metric of comparison for the HSI-derived CI. This instrument uses six light-emitting diodes (emitting light at 370, 470, 525, 570, 590, and 610 nm) which interact with phytoplankton in the water. Abundances of different phytoplankton groups (green algae, bluegreen algae, diatoms, and cryptophyta) are estimated by comparing the retrieved fluorescence excitation spectra to algal group-specific standard curves (Beutler et al., 2002).

The FluoroProbe was deployed by hand over the side of MTRI's research vessel with a rope. After equilibriating just below the water's surface as the instrument warmed up, the instrument was allowed to descend slowly through the water column until it hit the lake bottom, at which point it was pulled up and out of the water. Data was extracted off the FluoroProbe into the bbe++ software (version 2.1; bbe-Moldaenke GmbH) where standard calibrations were applied in order to derive chlorophyll-a concentrations for each phytoplankton group from the fluorescence returns.

Ground-based radiometric data was also collected in 2015 and 2016 using a FieldSpec III spectroradiometer to compare with the HSI-derived surface reflectance. This instrument has a spectral range of 350–2500 nm and a data collection time of 0.1 s. Spectral data was collected through the RS3 software program (v6.4; ASD, Inc.) and analyzed using the ViewSpecPro software program (v6.2; ASD, Inc.).

Downwelling irradiance was measured by attaching a remote cosine receptor (RCR) to the FieldSpec III fiberoptic cable. Pointing the RCR straight up and avoiding any potential shadows, 10 spectral measurements were taken and averaged together. The radiance of the water's surface was measured following the NASA standard protocol (Mueller et al., 2003). An 8-degree foreoptic was attached to the fiberoptic cable and pointed at the water at approximately a 45° angle off-nadir to reduce specular reflection (Mobley, 1999). Radiance was measured approximately 1 m from the target at approximately 150° from the sun's position while avoiding shadows, sun glint, and floating debris (Mobley, 1999). Samples of 20–30 radiance spectra were collected and averaged together. Spectra were processed and extracted via ViewSpecPro and reflectance was calculated as the averaged radiance divided by the averaged irradiance. The reflectance of the parking lot was measured following the same protocol.


Fig. 3. Map showing the location of the Maumee Bay State Park parking lot and the location of the light weight portable radiometer (LPR: white square in inset). The LPR was approximately 150 m from Lake Erie.
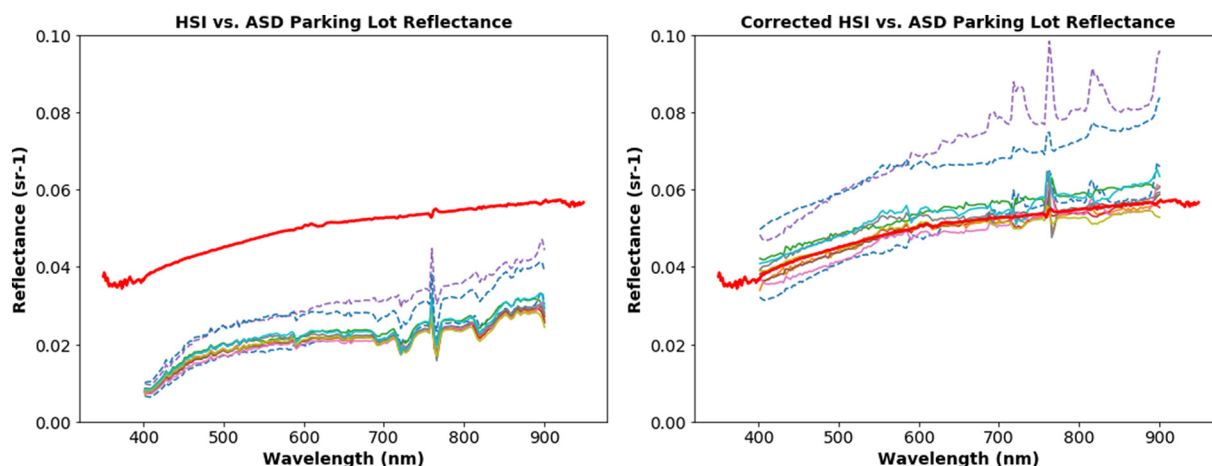
Fig. 4. NASA GRC HSI parking lot reflectance over the 2015 season. In situ reflectance from the ASD FieldSpec III is shown as a thick red line in both panels. Before correction (panel A), the HSI spectra exhibit uncharacteristically low reflectance relative to the ground-truth and are spectrally misshaped. After correction (panel B), the HSI spectra group well around the in situ reflectance spectra with the exception of 2 of the 3 cloudy days (shown as dashed lines).

In an effort to more rigorously monitor changes in the MBSP parking lot reflectance over long and short time scales to evaluate its viability as a long-term site for vicarious atmospheric correction of airborne HSI data, a hyperspectral lightweight portable radiometer (LPR) system was deployed in 2017 at the MBSP parking lot. This system used two OceanOptics STS (https://oceanoptics.com/product-category/sts-series/) sensors mounted to a pole to measure upwelling radiance and downwelling irradiance at wavelengths from 350 to 800 nm with 1.5 nm spectral resolution. Measurements were made once per minute during daylight hours for the duration of the field season. The device
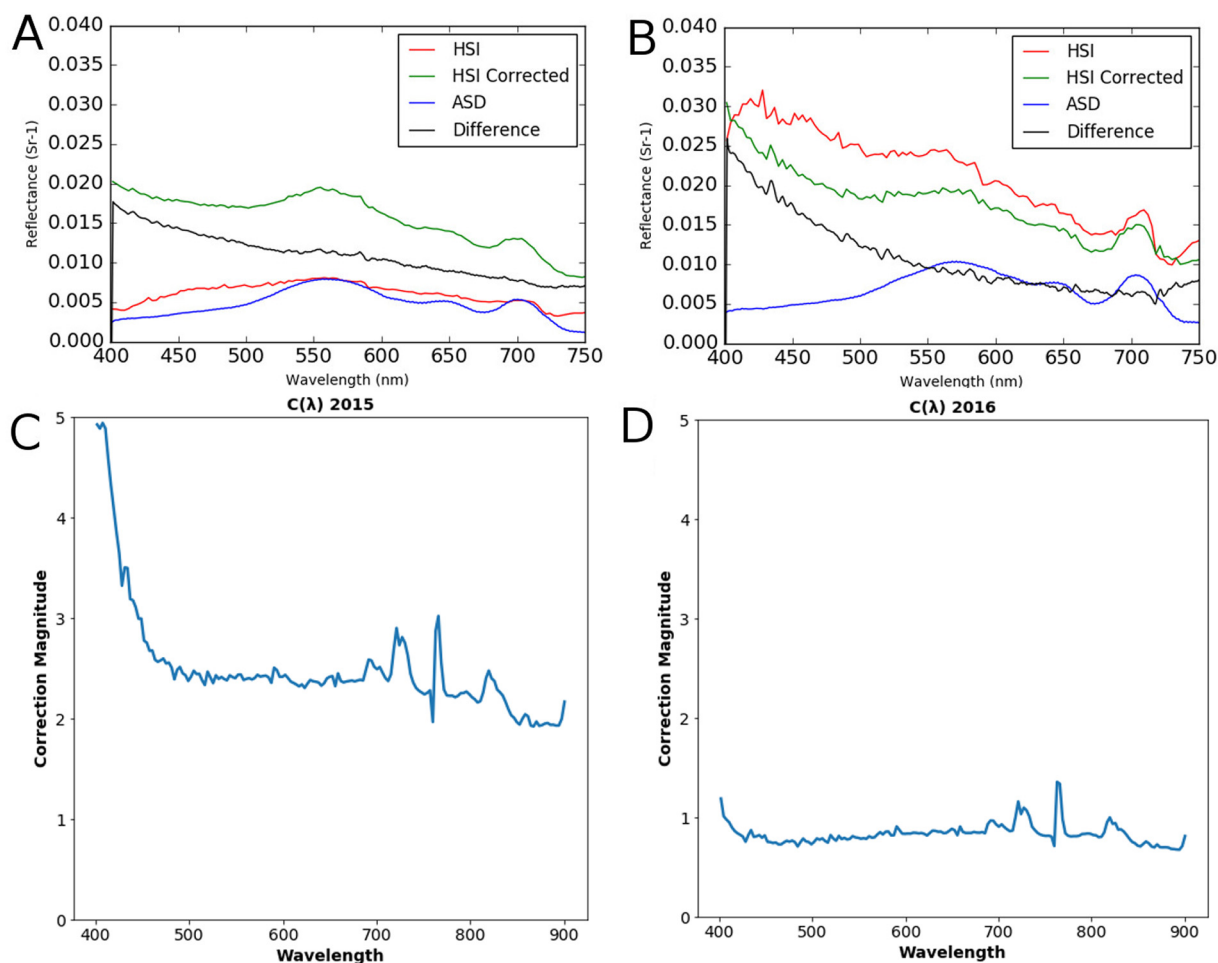
Fig. 5. Typical aquatic spectra are shown from 2015 (A) and 2016 (B), including in situ spectra from the ASD FieldSpec III and airborne data from the HSI system (before and after correction). The Difference line (in black) is the corrected HSI signal minus the ASD signal. Correction factors from 2015 (C) and 2016 (D) are also shown. Note that the 2016 correction factor is largely flat and of much lower magnitude than the 2015 correction factor.

was solar powered and communicated back to MTRI using a cellular network connection. Data was logged on the device using a SQlite3 database so data was preserved even during network failures. The STS sensors were relatively calibrated to the FieldSpec III using a 99% reflective Spectralon panel and a halogen lamp source in a dark room. Fig. 3 shows the location of the MBSP parking lot and its proximity to Lake Erie as well as the location of the LPR.

Results

MBSP parking lot reflectance derived from the HSI instrument were collected on various dates in July, August and September 2015 before (Fig. 4, panel A) and after (panel B) application of the vicarious correction routine (using one correction for all flights within the same year), as well as an in situ ASD measurement of the MBSP parking lot collected on August 3, 2015 (shown as a thick red line). The HSI reflectance exhibits significantly lower reflectance compared to the ASD field measurement (Fig. 4A). Additionally, the uncorrected HSI data shows a lack of sensitivity in the blue (<500 nm) wavelengths, and the HSI reflectance in general retains strong atmospheric absorption features, i.e., the prominent vertical features around 700 nm. In Fig. 4B, despite using a single correction factor across the wide range of dates observed, the corrected HSI data shows strong agreement with the single field measurement. Cloudy days are labeled using dashed lines, two out of three such days were the only data sets to widely disagree with the field-truth data with magnitudes well above the rest.

To confirm the efficacy of the vicarious correction factor when applied to aquatic targets, MTRI compared HSI corrected and uncorrected reflectance to same-day in situ measurements observed using the ASD

FieldSpec III. Typical spectra for ASD, uncorrected HSI, corrected HSI, and the difference between corrected HSI and ASD for 2015 and 2016 are shown in Fig. 5(A, B). The vicarious correction factors are shown in Fig. 5(C, D) for 2015 and 2016 respectively, with the difference in shape and magnitude between years due to instrument recalibration and reconfiguration of system components. The corrected HSI measurements show higher reflectance magnitudes than the ASD measured reflectance in both 2015 and 2016. However, the 2016 correction factor typically reduces the reflectance measurement; whereas the 2015 correction factor typically raises the reflectance compared to uncorrected data. Also of note, the uncorrected 2015 HSI reflectance is typically well matched with the ASD in magnitude but not shape, while the uncorrected 2016 HSI reflectance is typically much higher in magnitude but better matched in shape. Correspondingly, the 2015 correction factor dramatically improves spectral shape, while the 2016 correction factor has little effect on the shape except for low wavelengths (<450 nm).

The time series of data collected by the MBSP LPR system (Fig. 6) shows day-to-day variability of the parking lot spectra but no obvious long term trend. The spectra is sampled at three wavelengths, 450 nm, 530 nm, and 667 nm (blue, green, and red respectively). The three reference wavelength retrievals co-vary to a high degree. Pairwise Spearman's correlation tests indicate $r = 0.989$ for blue-green, $r = 0.934$ for blue-red, and $r = 0.958$ for green-red. Data from four days (July 2, 4, 9 and September 5, 2017) were excluded because they were not representative of parking lot spectra, which appear as vertical lines in Fig. 6 due to significant variability in the reflectance measurements. The blue and green band retrievals were found to be stable throughout the season using a median-based non-parametric regression (Thiel, 1950; Sen, 1968) with p-values of 0.61 and 0.95,
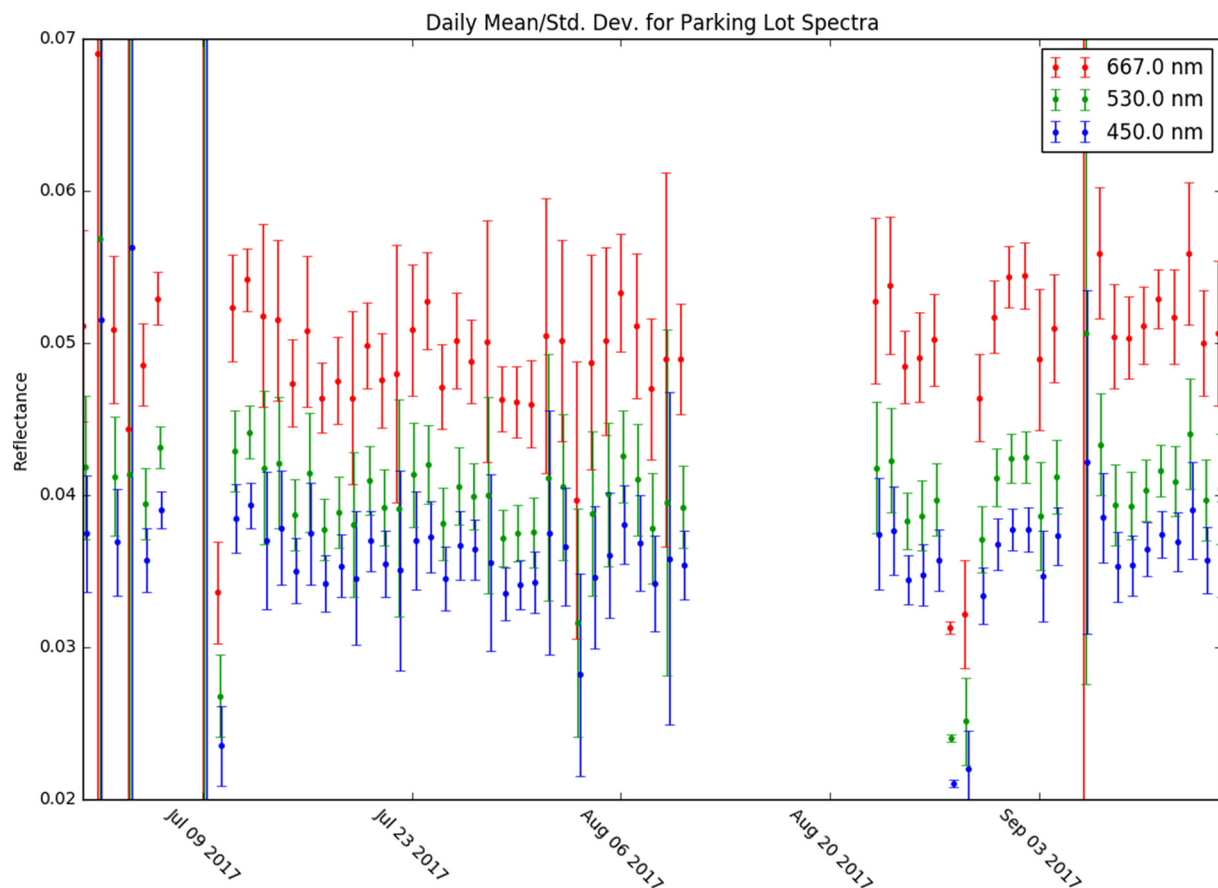
Fig. 6. Daily variability of MBSP parking lot reflectance, including mean and standard deviation error bars, for 3 reference wavelengths (450 nm, 530 nm, and 667 nm are colored as blue, green, and red, respectively). The extreme intra-day variance events (dates where the vertical bars extend outside the range of the plot) are likely caused by anomalous events, such as cars, people, or animals passing under the sensor. Days with low mean reflectance values in July and late August are indicative of wet pavement due to rain.

respectively. The red band reflectance significantly increased through the season ($p = .01$) but at a rate of only 0.000028 Sr^{-1} per day.

The culmination of the automated processing systems digesting HSI data are the colorized map outputs. For every flight track of data generated, both CI and SSI maps are created with a generic colorization scheme to convey the cyanoHABs severity in order to be easily understandable for stakeholders. As seen in Fig. 7, the HSI swath produces local but extremely high resolution images: at approximately half a kilometer across, depending on altitude, the entire cross-track FOV of the HSI swath represents less than half of a pixel from MODIS AQUA imagery. In the flight track processed with CI (Fig. 7A), a boat wake is visible as a loop of lower CI concentration near the middle of the image, caused by the boat propeller mixing the water column, thus demonstrating the stratified nature of heavy cyanobacterial blooms. The flight track processed with SSI (Fig. 7B) also shows the often sharp boundaries between scum and non-scum conditions.

Over the 2015 field season, 16 matchups were found where there were in situ FluoroProbe retrievals and HSI imagery for the same site on the same day and the results were utilized to generate the scatterplot in Fig. 8. These 16 matchups were spread throughout the basin and across the season, representing the range of conditions seen in WBLE. In Fig. 8, the x-axis is the HSI-derived CI index value, which has traditionally been related to cell counts (Stumpf et al., 2012). The y-axis is the FluoroProbe-derived bluegreen algal (cyanobacteria) concentration in mg/m^3. An R^2 coefficient of 0.72 was generated indicating a strong relationship between HSI-derived CI and FluoroProbe-derived bluegreen algae concentration. The SSI algorithm was not validated in this study due to insufficient in situ scum observations coincident with aircraft overflights, but this algorithm was extensively validated in WBLE showing a 93% surface scum classification accuracy (Sayers et al., 2016).

Case Study 1: Ohio River, September 3, 2015

One of the primary advantages of the HSI system is the high spatial resolution, which means the system is capable of monitoring small freshwater systems such as inland lakes or rivers that would normally be beyond the resolving capabilities of space-based platforms. In this cases study, the EPA had reports of potential cyanobacterial presence, but was unsure of the extent or severity of the bloom. The derived CI products (Fig. 9) revealed cyanobacteria presence in three municipalities along the river, including Miller, OH (A), Proctorville, OH (B) and Huntington, KY (C). Of these the most extensive was Proctorville, which showed clear indications of cyanobacteria bloom patterning flowing downriver. The brighter green colors represent higher CI values. In this case, significant cyanobacteria presence is depicted by streaks of bright green. The Ohio EPA found these results particularly useful in their water quality management decision making process (pers. comm., John Lekki, NASA Glenn Research Center). This cyanoHAB presence in the Ohio River would not have been detected using the 1 km resolution MODIS satellite data and there is no guarantee that a satellite with higher spatial resolution would have flown over the river while the bloom was present (according to USGS EarthExplorer, Landsat-7 flew over the region on September 6, Landsat-8 flew over on September 7, and Sentinel-2 did not fly over the region within 5 days of the HSI overflight).

Case Study 2: Toledo Water Intake, July 27, 2015

Monitoring potential cyanoHAB presence in the vicinity of water intakes in Lake Erie was an important element of the NASA GRC HSI system. This monitoring potential is demonstrated by the results of the
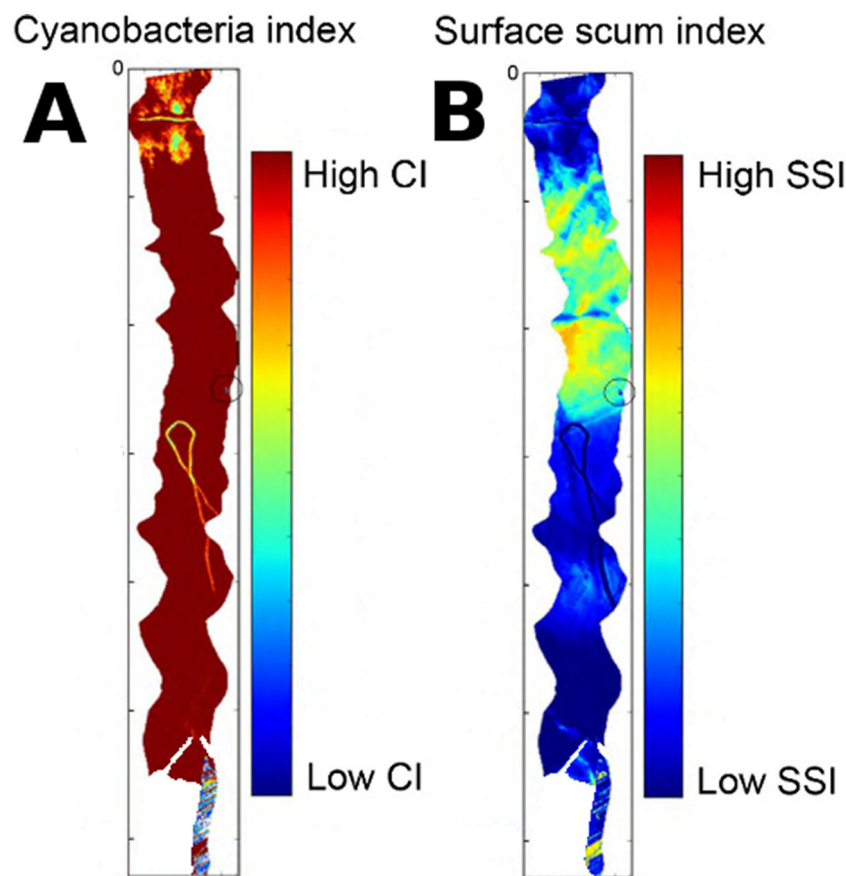
Fig. 7. NASA Glenn Research Center HSI tracks from August 10, 2015 near the Toledo Water Intake processed with CI (A) and SSI (B) showing the spatial variability of algal blooms and surface scums. The high resolution of the HSI imagery reveals details that would be obscured by space-based observation platforms. The Toledo Water Intake is shown in both tracks as a black circle.

July 27, 2015 overflight of the Toledo Water Intake. This intake provides drinking water for more than one million people, and was central to the Toledo water crisis in which the water supply was contaminated with toxins produced by cyanobacteria (Jetoo et al., 2015). Fig. 10 shows the HSI-derived CI maps (green and black strips) overlaid on the MODIS-derived algal bloom extent (orange pixels) produced by MTRI. The location of the Toledo Water Intake is indicated as a red dot on the figure. The 1 km resolution MODIS cyanoHAB data show the general extent of the bloom, but do not show sufficient detail of the cyanoHABs extent in the proximity of the Toledo Water Intake. In contrast, the HSI track shows the water intake is in a region of low to moderate cyanoHAB presence, but that higher concentration blooms (shown as brighter green in the figure) are in close proximity (~500–1000 m) to the intake.

Discussion

Methodology to generate near-real time (within 24 h) cyanoHAB mapping products from high resolution airborne remote sensing data has been developed and tested using the NASA GRC HSI data collected over Lake Erie and the Ohio River. Near-real time water quality monitoring protocols using airborne remote sensing data are not well reported in the literature due to the difficulty standardizing airborne data over many flights. Quantification and correction of atmospheric effects are a significant challenge to overcome in airborne water remote sensing and are typically quantified using coincident in situ radiometric observations. While this approach works well for a single flight, it is generally cost and time prohibitive to make in situ measurements for many flights in a routine operational application. The vicarious correction approach using a persistent and well characterized target (i.e. the parking lot at Maumee Bay State Park) in close proximity to the area of interest (i.e. WBLE), can allow for the correction of many images from many days to be corrected provided the calibration target is imaged each day. An

additional advantage of this approach is that it accounts for sensor system variability along with atmospheric contribution.

The vicarious correction methodology utilized to correct HSI data generally performed well, but there are still some unresolved issues. For instance, Fig. 4 shows how cloud cover can impact the HSI reflectance retrievals, even after correction. One potential cause of this issue is the infrequency of irradiance measurements gathered by the HSI system. On days with varying cloud cover, this can result in significant error when the surface conditions at a given point in the swath are mismatched with the relative position of clouds and the aircraft at the time of measurement. This issue would be less a concern on days with total cloud cover as the illumination would be consistently low across the imaged area. As seen in Fig. 4, this results in increased reflectance magnitude after the vicarious correction is applied but the spectral shape remains mostly similar. This magnitude shift would be problematic for analytical and semi-analytical algorithms, but shape-based algorithms are less impacted by this issue. This finding suggests that while the airborne system does have the advantage of being able to view water conditions under cloud cover, caution needs to be used on days with intermittent cloud cover.

Another issue is with the impact of diffuse sky and sun glint on reflectance retrievals over water. The diffuse sky influence can be seen in Fig. 5 where the shape of the corrected HSI observation does not match ASD measurements, unlike what was observed in the parking lot comparisons (Fig. 4). The two spectra share a similar shape between the 500–750 nm wavelengths, but in the blue bands the ASD shows a gradual increase in reflectance from 400 to 500 nm while the corrected HSI shows a local peak at 400 nm and a gradual decrease from 400 to 500 nm. This shape difference accounts for the bulk of the HSI error (represented by the black 'Difference' line in Fig. 5) which is highest in the blue wavelengths but levels off between 500 and 750 nm. Neither dataset was corrected for diffuse sky contamination, but the ASD viewing angle was optimized by the operating personnel so the diffuse sky
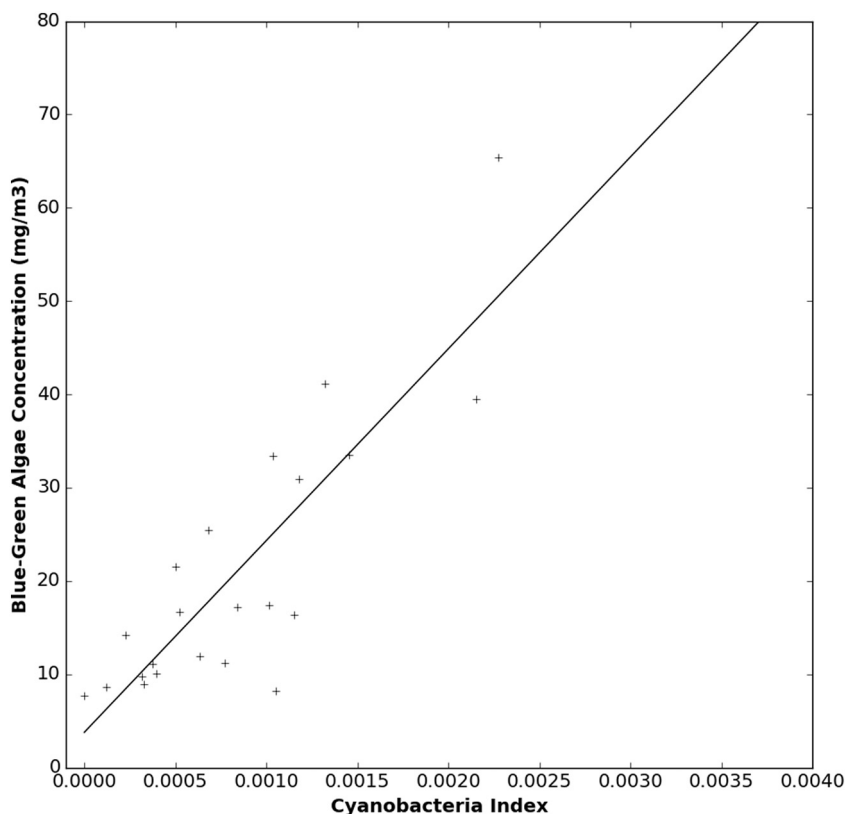

Fig. 8. 2015 comparison of HSI-derived CI values (x-axis) and in situ blue-green algae concentrations (y-axis) from the same site on the same day show a strong correlation between CI values and field measured cyanobacterial abundance ($R^2 = 0.72$).

candidate as a calibration target for airborne remote sensing measurements of western Lake Erie.

Using the LPR to collect persistent, long-term measurements of a stable target removes the expense of sending a field crew out to collect radiometric measurements of a calibration target during each flight. This approach would likely work in other scenarios as well, but a concerted effort to assess the stability of the target is important. For instance, a grassy field near the study area may provide a reference similar to a surface scum, but such a target is neither spectrally homogenous nor Lambertian-like, two characteristics of an ideal calibration target (Smith and Milton, 1999). If no viable stable target is available near the target, a more standard calibration approach would be necessary in which a calibration target such as a tarp or mirror array is brought to the sampling location.

The case studies presented demonstrate the utility of near-real time airborne hyperspectral data products for water resource managers and other stakeholders. While the smaller geographic coverage of airborne sensors limits the ability to use it for fully monitoring large lakes, airborne remote sensing systems such as the HSI allow for the targeted monitoring of important areas (i.e., water intakes) and small water bodies potentially affected by cyanoHABs, independent of cloud cover and spatial size. The fine spatial resolution of the HSI system allows for the capture of fine spatial variability as seen in Figs. 7 and 9 and the ability to collect data on demand allows for rapid response to bloom events. The hyperspectral nature of the instrument allows for the application of any water quality monitoring algorithm to the data, though the impact of atmospheric and diffuse sky contamination should play a role in selecting algorithms. The near-real time processing methodology described above and the Ohio River case study demonstrate the ability of the system to be used for rapid response monitoring of cyanoHAB events. The latest version of the HSI sensor (HSI3) has a wider swath, potentially making it feasible to fully map large areas such as the Western Basin of Lake Erie using overlapping flight lines.

The demonstrated methodology which includes geometric, radiometric, and vicarious corrections, and derived product generation in near-real time can be utilized by other aircraft and unmanned aerial vehicle (UAV) remote sensing systems.

Conclusions and recommendations

The NASA GRC HSI system is a high resolution hyperspectral imager capable of generating quality radiance data and a reasonable estimate of reflectance after implementing vicarious corrections. Coupled with the CI and SSI algorithms, which are easy to implement and automate, this allows for the near-real time (within 24 h) processing of large quantities of data gathered in a given flight. The flexible nature of aircraft deployment (i.e. flight line location, under cloud operation) combined with the high resolution and rapid analysis provides unique insights into water quality conditions not offered by space-based solutions. While the cost of deployment and limited spatial coverage of airborne remote sensing limit the ability to do daily monitoring of large lakes, this is an effective tool for long-term weekly monitoring of targeted areas including water intakes and smaller water bodies while also allowing for on-demand deployments to capture bloom events in progress. This approach is not meant to replace the use of satellite remote sensing which can provide valuable region-wide context. Rather, it is meant as a complementary dataset to aid in the monitoring of cyanoHABs at scales not easily or effectively monitored by existing systems.
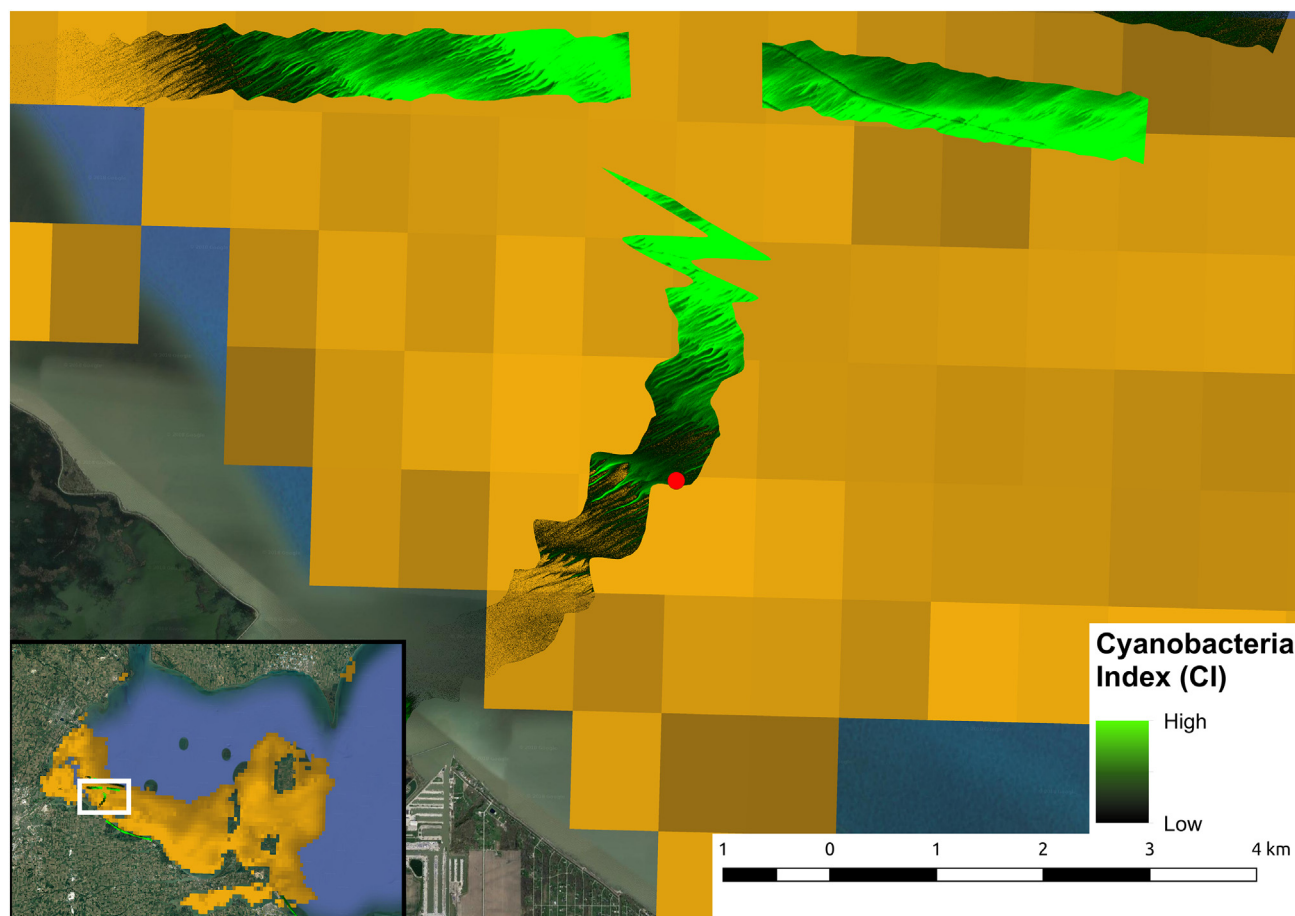
Fig. 10. NASA GRC HSI tracks (colored on a scale of dark to bright green based on HSI-derived CI) overlain on MTRI MODIS cyanoHAB mapping product (colored in orange) on July 27, 2015. The Toledo Water Intake is shown as a red dot.

The vicarious correction technique adequately converted at-sensor HSI reflectance to surface reflectance. Future work will focus on implementing a correction for diffuse sky reflectance to isolate the aquatic contribution to spectra. This will play a vital role in the applicability of bio-optical algorithms, such as the CPA-A (Shuchman et al., 2013), QAA (Lee et al., 2009), and GIOP (Werdell et al., 2013) which retrieve inherent optical properties of water, but are less robust to diffuse sky contamination than simpler shape-based algorithms such as the CI or SSI. Further work should also investigate the use of phytoplankton and cyanobacteria pigment absorption and scattering features to potentially assess species and size distributions to take advantage of the hyperspectral nature of the sensor. Additionally, this could allow for the early detection of cyanoHAB events which is currently not possible using the CI approach.

Acknowledgements

References

Ackerman, S.A., Heidinger, A., Foster, M.J., Maddux, B., 2013. Satellite regional cloud climatology over the Great Lakes. Remote Sens. 5 (12), 6223–6240.
Beck, R., Zhan, S., Liu, H., Tong, S., Yang, B., Xu, M., Ye, Z., Huang, Y., Shu, S., Wu, Q., Wang, S., Berling, K., Murray, A., Emery, E., Reif, M., Harwood, J., Young, J., Nietch, C., Macke, D., Martin, M., Stillings, G., Stumpf, R., Su, H., 2016. Comparison of satellite reflectance algorithms for estimating chlorophyll-a in a temperate reservoir using coincident hyperspectral aircraft imagery and dense coincident surface observations. Remote Sens. Environ. 178, 15–30.
Beck, R., Xu, M., Zhan, S., Liu, H., Johansen, R.A., Tong, S., Yang, B., Shu, S., Wu, Q., Wang, S., Berling, K., Murray, A., Emery, E., Reif, M., Harwood, J., Young, J., Martin, M., Stillings, G., Stumpf, R., Su, H., Ye, Z., Huang, Y., 2017. Comparison of satellite reflectance algorithms for estimating Phycocyanin values and cyanobacterial Total biovolume in a temperate reservoir using coincident hyperspectral aircraft imagery and dense coincident surface observations. Remote Sens. 9 (6), 538.
Beutler, M., Wiltshire, K.H., Meyer, B., Moldaenke, C., Lüring, C., Meyerhöfer, M., Hansen, U.P., Dau, H., 2002. A Fluorometric method for the differentiation of algal populations in vivo and in situ. Photosynth. Res. 72 (1), 39–53.
Bianchi, T.S., Engelhaupt, E., Westman, P., Andren, T., Rolff, C., Elmgren, R., 2000. Cyanobacterial blooms in the Baltic Sea: natural or human-induced? Limnol. Oceanogr. 45 (3), 716–726.
Binding, C.E., Greenberg, T.A., Bukata, R.P., 2013. The MERIS maximum chlorophyll index; its merits and limitations for inland water algal bloom monitoring. J. Great Lakes Res. 39, 100–107.
Bosse, K.R., Sayers, M.J., Shuchman, R.A., Fahnenstiel, G.L., Ruberg, S.A., Fanslow, D.L., Stuart, D.G., Johengen, T.H., Burtner, A.M., 2018. Spatial-temporal variability of cyanobacteria vertical structure in Western Lake Erie: implications for remote sensing observations. Journal of Great Lakes Research, this issue.
Boyer, G.L., 2007. The occurrence of cyanobacterial toxins in New York lakes: lessons from the MERHAB-lower Great Lakes program. Lake and Reservoir Management 23 (2), 153–160.
Brando, V.E., Dekker, A.G., 2003. Satellite hyperspectral remote sensing for estimating estuarine and coastal water quality. IEEE Trans. Geosci. Remote Sens. 41 (6), 1378–1387.
Codd, G.A., Morrison, L.F., Metcalf, J.S., 2005. Cyanobacterial toxins: risk management for health protection. Toxicol. Appl. Pharmacol. 203 (3), 264–272.
Dall'Olmo, G., Gitelson, A.A., 2005. Effect of bio-optical parameter variability on the remote estimation of chlorophyll-a concentration in turbid productive waters: experimental results. Appl. Opt. 44, 412–422.
Gitelson, A.A., Gritz, U., Merzlyak, M.N., 2003. Relationships between leaf chlorophyll content and spectral reflectance and algorithms for non-destructive chlorophyll assessment in higher plant leaves. J. Plant Physiol. 160, 271–282.
Ho, J.C., Stumpf, R.P., Bridgeman, T.B., Michalak, A.M., 2017. Using Landsat to extend the historical record of lacustrine phytoplankton blooms: a Lake Erie case study. Remote Sens. Environ. 191, 273–285.
Ibelings, B.W., Vonk, M., Los, H.F., van der Molen, D.T., Mooij, W.M., 2003. Fuzzy modeling of cyanobacterial surface waterblooms: validation with NOAA-AVHRR satellite images. Ecol. Appl. 13 (5), 1456–1472.

Jetoo, S., Grover, V.I., Krantzberg, G., 2015. The toledo drinking water advisory: suggested application of the water safety planning approach. Sustainability 7 (8), 9787–9808.
Joehnk, K.D., Huisman, J.E.F., Sharples, J., Sommeijer, B.E.N., Visser, P.M., Stroom, J.M., 2008. Summer heatwaves promote blooms of harmful cyanobacteria. Glob. Chang. Biol. 14 (3), 495–512.
Kanoshina, I., Lips, U., Leppänen, J.M., 2003. The influence of weather conditions (temperature and wind) on cyanobacterial bloom development in the Gulf of Finland (Baltic Sea). Harmful Algae 2 (1), 29–41.
Klemer, A.R., Cullen, J.J., Mageau, M.T., Hanson, K.M., Sundell, R.A., 1996. Cyanobacterial buoyancy regulation: the paradoxical roles of carbon. J. Phycol. 32 (1), 47–53.
Lee, Z., Lubac, B., Werdell, J., & Arnone, R., 2009. An Update of the Quasi-Analytical Algorithm (QAA_v5). International Ocean Color Group Software Report, 1-9.
Lekki, J., Anderson, R., Nguyen, Q. V., Demers, J., Leshkevich, G., Flatico, J., & Kojima, J., 2009. Development of Hyperspectral remote sensing capability for the early detection and monitoring of Harmful Algal Blooms (HABs) in the Great Lakes. AIAA Infotech@Aerospace Conference and AIAA Unmanned. Unlimited Conference.
Lekki, J., Anderson, R., Avouris, D., Becker, R., Churnside, J., Cline, M., Demers, J., Leshkevich, G., Liou, L., Luvall, J., Ortiz, J., Royce, A., Ruberg, S., Sawtell, R., Sayers, M., Schiller, S., Shuchman, R., Simic, A., Stuart, D., Sullivan, P., Tavernelli, P., Tokars, R., Vander Woude, A., 2017. Airborne Hyperspectral Sensing of Monitoring Harmful Algal Blooms in the Great Lakes Region: System Calibration and Validation. Report NASA/TM-2017-219071.
Lekki, J., Deutsch, E., Sayers, M., Bosse, K., Anderson, R., Tokars, R., 2018. Determining remote sensing spatial resolution requirements for the monitoring of harmful algal blooms in the Great Lakes. Journal of Great Lakes Research, this issue.
Melstrom, R.T., Lupi, F., 2013. Valuing recreational fishing in the Great Lakes. N. Am. J. Fish Manag. 33 (6), 1184–1193.
Mishra, S., Mishra, D.R., 2012. Normalized difference chlorophyll index: a novel model for remote estimation of chlorophyll-a concentration in turbid productive waters. Remote Sens. Environ. 117, 394–406.
Mobley, C.D., 1999. Estimation of the remote-sensing reflectance from above-surface measurements. Appl. Opt. 38 (36), 7442–7455.
Mobley, C.D., Werdell, J., Franz, B., Ahmad, Z., Bailey, S., 2016. Atmospheric Correction for Satellite Ocean Color Radiometry. NASA Tech. Memo 217551.
Mueller, J.L., Fargion, G.S., McClain, C.R., 2003. Ocean Optics Protocols for Satellite Ocean Color Sensor Validation, Revision 4. Radiometric Measurements and Data Analysis Protocols. NASA Tech. Memo, Volume III, p. 21621.
Ortiz, J.D., Avouris, D., Schiller, S., Luvall, J.C., Lekki, J.D., Tokars, R.P., Anderson, R.C., Shuchman, R., Sayers, M., Becker, R., 2017. Intercomparison of approaches to the empirical line method for vicarious hyperspectral reflectance calibration. Front. Mar. Sci. 4, 296.
Paerl, H.W., Hall, N.S., Calandrino, E.S., 2011. Controlling harmful cyanobacterial blooms in a world experiencing anthropogenic and climatic-induced change. Sci. Total Environ. 409 (10), 1739–1745.
Qin, B., Zhu, G., Gao, G., Zhang, Y., Li, W., Paerl, H.W., Carmichael, W.W., 2010. A drinking water crisis in Lake Taihu, China: linkage to climatic variability and Lake management. Environ. Manag. 45 (1), 105–112.
Rapala, J., Sivonen, K., Lyra, C., Niemelä, S.I., 1997. Variation of microcystins, cyanobacterial Hepatotoxins, in Anabaena spp. as a function of growth stimuli. Appl. Environ. Microbiol. 63 (6), 2206–2212.
Robarts, R.D., Zohary, T., 1987. Temperature effects on photosynthetic capacity, respiration, and growth rates of bloom-forming cyanobacteria. N. Z. J. Mar. Freshw. Res. 21 (3), 391–399.
Rowe, M.D., Anderson, E.J., Wynne, T.T., Stumpf, R.P., Fanslow, D.L., Kijanka, K., Vanderploeg, H.A., Strickler, J.R., Davis, T.W., 2016. Vertical distribution of buoyant Microcystis blooms in a Lagrangian particle tracking model for short-term forecasts in Lake Erie. Journal of Geophysical Research: Oceans 121 (7), 5296–5314.
Sayers, M., Fahnenstiel, G.L., Shuchman, R.A., Whitley, M., 2016. Cyanobacteria blooms in three eutrophic basins of the Great Lakes: a comparative analysis using satellite remote sensing. Int. J. Remote Sens. 37 (17), 4148–4171.
Schindler, D.W., Hecky, R.E., McCullough, G.K., 2012. The rapid eutrophication of Lake Winnipeg: greening under global change. J. Great Lakes Res. 38, 6–13.
Sen, P.K., 1968. Estimates of the regression coefficient based on Kendall's tau. J. Am. Stat. Assoc. 63 (324), 1379–1389.
Shuchman, R.A., Leshkevich, G., Sayers, M.J., Johengen, T.H., Brooks, C.N., Pozdnyakov, D., 2013. An algorithm to retrieve chlorophyll, dissolved organic carbon, and suspended minerals from Great Lakes satellite data. J. Great Lakes Res. 39, 14–33.
Sivonen, K., 1996. Cyanobacterial toxins and toxin production. Phycologia 35 (6S), 12–24.
Smith, G.M., Milton, E.J., 1999. The use of the empirical line method to calibrate remotely sensed data to reflectance. Int. J. Remote Sens. 20 (13), 2653–2662.
Stumpf, R.P., Wynne, T.T., Baker, D.B., Fahnenstiel, G.L., 2012. Interannual variability of cyanobacterial blooms in Lake Erie. PLoS One 7 (8), e42444.
Stumpf, R.P., Davis, T.W., Wynne, T.T., Graham, J.L., Loftin, K.A., Johengen, T.H., Gossiaux, D., Palladino, D., Burtner, A., 2016. Challenges for mapping cyanotoxin patterns from remote sensing of cyanobacteria. Harmful Algae 54, 160–173.
Thiel, H., 1950. A rank-invariant method of linear and polynomial regression analysis, part 3, in: Proceedings of Koninalijke Nederlandse Akademie van Weinenschatpen A, Vol. 53. p. 1397-1412.
Urquhart, E.A., Schaeffer, B.A., Stumpf, R.P., Loftin, K.A., Werdell, P.J., 2017. A method for examining temporal changes in cyanobacterial harmful algal bloom spatial extent using satellite remote sensing. Harmful Algae 67, 144–152.
Vahtera, E., Conley, D.J., Gustafsson, B.G., Kuosa, H., Pitkänen, H., Savchuk, O.P., Tamminen, T., Viitasalo, M., Voss, M., Wasmund, N., Wulff, F., 2007. Internal ecosystem feedbacks enhance nitrogen-fixing cyanobacteria blooms and complicate management in the Baltic Sea. AMBIO: A Journal of the Human Environment 36 (2), 186–194.

van Rijn, J., Shilo, M., 1985. Carbohydrate fluctuations, gas vacuolation, and vertical migration of scum-forming cyanobacteria in fishponds. Limnol. Oceanogr. 30 (6), 1219–1228.

Werdell, P.J., Franz, B.A., Bailey, S.W., Feldman, G.C., Boss, E., Brando, V.E., Dowell, M., Hirata, T., Lavender, S.J., Lee, Z., Loisel, H., Maritorena, S., Mélin, F., Moore, T.S., Smyth, T.J., Antoine, D., Devred, E., d'Andon, O.H.F., Mangin, A., 2013. Generalized ocean color inversion model for retrieving marine inherent optical properties. Appl. Opt. 52 (10), 2019–2037.

Wynne, T.T., Stumpf, R.P., 2015. Spatial and temporal patterns in the seasonal distribution of toxic cyanobacteria in Western Lake Erie from 2002–2014. Toxins 7 (5), 1649–1663.

Wynne, T.T., Stumpf, R.P., Tomlinson, M.C., Warner, R.A., Tester, P.A., Dyble, J., Fahnenstiel, G.L., 2008. Relating spectral shape to cyanobacterial blooms in the Laurentian Great Lakes. Int. J. Remote Sens. 29 (12), 3665–3672.

Wynne, T.T., Stumpf, R.P., Tomlinson, M.C., Dyble, J., 2010. Characterizing a cyanobacterial bloom in Western Lake Erie using satellite imagery and meteorological data. Limnol. Oceanogr. 55 (5), 2025–2036.

Wynne, T.T., Stumpf, R.P., Briggs, T.O., 2013. Comparing MODIS and MERIS spectral shapes for cyanobacterial bloom detection. Int. J. Remote Sens. 34 (19), 6668–6678.

Zhao, D.Z., Xing, X.G., Liu, Y.G., Yang, J.H., Wang, L., 2010. The relation of chlorophylla concentration with the reflectance peak near 700 nm in algae-dominated waters and sensitivity of fluorescence algorithms for detecting algal bloom. Int. J. Remote Sens. 31, 39–48.